Pergamon

Geochimica et Cosmochimica Acta, Vol. 65, No. 10, pp. 1529–1543, 2001

0016-7037/01 $20.00 + .00

PII S0016-7037(01)00551-8

Prediction of trace metal partitioning between minerals and aqueous solutions: A linear free energy correlation approach

YIFENG WANG[1,*] and HUIFANG XU[2]

[1]Sandia National Laboratories, 4100 National Parks Highway, Carlsbad, NM 88220, USA
[2]Department of Earth and Planetary Sciences, Northrop Hall, University of New Mexico, Albuquerque, NM 87131, USA

(*Received May* 4, 2000; *accepted in revised form November* 2, 2000)

Abstract—Trace metal partitioning between authigenic minerals and aqueous solutions is of great interest to both geochemical and environmental communities. In this paper, we have developed a linear free energy correlation model that correlates metal partition coefficients with metal cation properties:

$$-2.303\ RT\ \log K_d + \Delta G^{o}_{f,M^{z+}} = a^{*}_{M_H X}\Delta G^{o}_{n,M^{z+}} + \beta^{*}_{M_H X} r_{M^{z+}} + b^{*}_{M_H X}$$

where $a^{*}_{M_H X}$, $\beta^{*}_{M_H X}$, and $b^{*}_{M_H X}$ are constants, which can be determined by a regression analysis. For isovalent metal partitioning, because of the constraint of $K_d = 1$ for the host metal, this correlation can be also expressed as:

$$-2.303\ RT\ \log K_d = a^{*}_{M_H X}(\Delta G^{o}_{n,M^{z+}} - \Delta G^{o}_{n,M_H^{z+}}) + \beta^{*}_{M_H X}(r_{M^{z+}} - r_{M_H^{z+}}) - (\Delta G^{o}_{f,M^{z+}} - \Delta G^{o}_{f,M_H^{z+}}).$$

Host minerals from an isostructural family have the same linear free energy relationship, as long as the relationship is expressed as a function of the differences in cation properties between substituent and host metals. We have applied our model to both isovalent and non-isovalent metal partitioning in carbonate minerals. The model closely fits experimental data, demonstrating the robustness of the proposed linear free energy relationship. Using the model, we have predicted the partition coefficients of divalent and trivalent metals between various carbonate minerals and aqueous solutions. The differences between the predicted and experimental values are generally less than 1 logarithmic unit for divalent cations and less than 0.4 logarithmic unit for trivalent cations. Magnesite is predicted to have the largest partition coefficients among the carbonate minerals with a calcite structure and therefore, can be a good scavenger for toxic metals. The kinetic effect on metal partitioning can be described graphically by a "seesaw" line anchored at a host cation. To explain the rate dependence of partition coefficients, we have proposed a conceptual model that relates metal partitioning to surface adsorption. The conceptual model suggests that as the rate of host mineral precipitation increases, the ratio of substituent to host cation in a solid approaches what is in the adsorbed layer. The linear free energy correlation model developed in this paper provides a useful tool for systematizing the existing experimental data and for predicting unknown partition coefficients.

1. INTRODUCTION

Trace metal partitioning between authigenic minerals and aqueous solutions is of great interest to both geochemical and environmental communities. In the studies of sedimentary rock diagenesis, the contents of trace metals in authigenic minerals such as calcium carbonates are commonly used to infer the chemistry of diagenetic pore fluids (e.g., Meyers, 1974, 1978; Grover and Read, 1983; Veizer, 1983). For instance, the variations of Mn^{2+} and Fe^{2+} contents in calcite, which can be easily detected by cathodoluminescence, may reflect redox condition changes in diagenetic environments (Frank et al., 1982; Barnaby and Rimstidt, 1989). From an environmental perspective, coprecipitation of toxic metals with authigenic minerals plays an important role in retarding contaminant migration in natural environments (e.g., Davis et al., 1987; Tesoriero and Pankow, 1996). As compared to surface adsorption, coprecipitation essentially "freezes" toxic metals in host mineral structures and therefore, greatly reduces the chance for metal remobilization. Coprecipitation is also considered to be important to the containment of radioactive wastes in geologic repositories (Curti, 1997, 1999).

Enormous efforts have been made on experimental determination of partition coefficients (K_d) (e.g., Lorens, 1981; Mucci and Morse, 1983; Veizer, 1983; Dromgoole and Walter, 1990; Zhong and Mucci, 1995; Tesoriero and Pankow, 1996). An excellent compilation of K_d values of divalent and trivalent metals in carbonate minerals can be found in Rimstidt et al. (1998) and Curti (1997, 1999). It has been observed that the partition coefficients of divalent metals in calcite can either increase or decrease with host mineral precipitation rates, depending on whether their values are <1 or >1 (Lorens 1981; Dromgoole and Walter, 1990; Tesoriero and Pankow, 1996).

Several thermodynamic models have been developed on trace metal partitioning into minerals (e.g., McIntire, 1963; Sverjensky, 1984, 1985; Blundy and Wood, 1994; Purton et al., 1995; Gnanapragasam and Lewis, 1995; Blundy et al., 1996; Rimstidt et al., 1998). Notably, Sverjensky (1984, 1985) has developed a linear free energy correlation model that correlates metal partition coefficients with the Gibbs free energies of formation of corresponding metal cations. This approach is appealing, because it is able to predict metal partition coefficients for which no experimental data are available. However,

*Author to whom correspondence should be addressed (ywang@sandia.gov).

because the model does not include the effect of cation radii, its application is limited to cations with similar radii (Sverjensky, 1984). In fact, the effect of cation radii can have a significant contribution to overall metal partitioning (Gnanapragasam and Lewis, 1995; Rimstidt et al., 1998, Fig. 5). Similarly, Rimstidt et al., (1998) have correlated metal partition coefficients for carbonate minerals with the solubility products of pure metal carbonate phases. This model is currently limited by the lack of appropriate mineral solubility product data. For instance, large divalent cations such as Pb^{2+}, Ra^{2+}, Ba^{2+}, Sr^{2+}, Sn^{2+}, and Eu^{2+} never form stable carbonate minerals with a calcite structure (Speer, 1983). The solubility products of these "fictitious" mineral phases are difficult to obtain. Finally, there are other types of metal partitioning models that explicitly account for the effect of lattice strain created by the difference of radii between substituent and host cations (Blundy and Wood, 1994; Purton et al., 1995; Gnanapragasam and Lewis, 1995; Blundy et al., 1996). These types of models were originally developed for mineral-melt systems. The partition coefficients of metals between a mineral and a coexisting melt can be related to the Young's modulus of the host mineral and the radius difference of cations (Blundy and Wood, 1994; Purton et al., 1995; Blundy et al., 1996). It may be difficult to directly apply these models to mineral-aqueous solution systems, but nevertheless, these models help us to gain insight into the effect of cation radii on metal partitioning.

In this paper, we want to demonstrate that metal partitioning between minerals and aqueous solutions is controlled by three factors: (1) the chemical bonding energies of substituent cations within a host mineral structure, (2) the excessive energies created by the size difference between substituent and host cations, and (3) the chemical potential difference between substituent and host cations in solutions. We will first develop a linear free energy correlation model to integrate these factors into a coherent theoretical framework. We will then use the model to systemize the existing experimental data and predict the partition coefficients of divalent and trivalent metals in carbonate minerals. Finally, a theoretical consideration of the rate dependence of partition coefficients will be presented.

2. LINEAR FREE ENERGY CORRELATION

The model developed in this paper is based on the linear free energy correlation established by Sverjensky and Molling (1992), which correlates the standard Gibbs free energies of formation ($\Delta G^0_{f,MX}$) of minerals within an isostructural family (MX) with the properties of the corresponding metal cations:

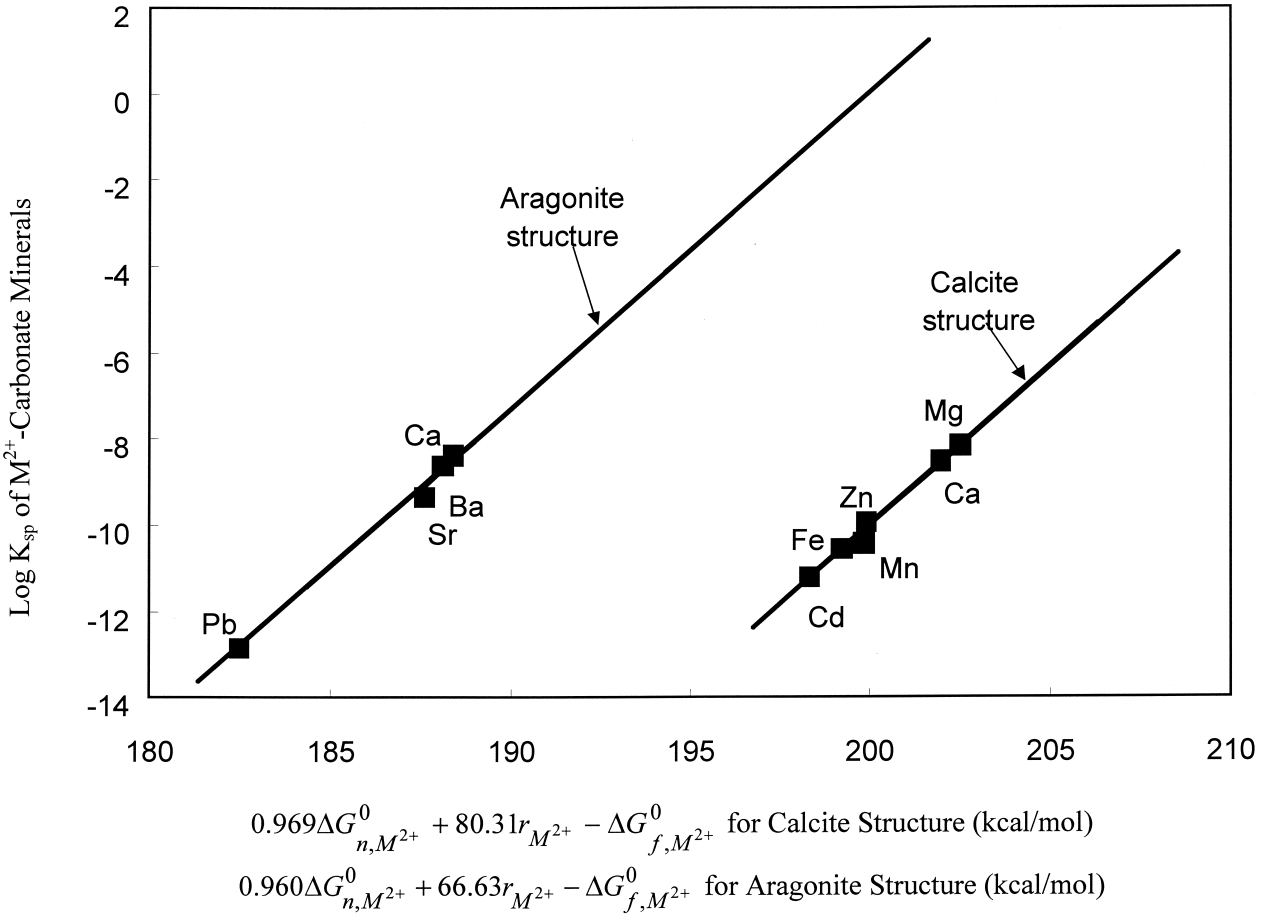

Fig. 1. Linear correlation of solubility products of divalent metal carbonate minerals with metal cation properties. The experimental Log K_{sp} values are calculated from Gibbs free energy data given in Sverjensky and Molling (1992) and Drever (1982).

Table 1. Summary of model parameters obtained by regression.

	a_{MX}	β_{MX} (kcal/mol/Å)	b'_{MX} (kcal/mol)
Pure divalent metal carbonate phases			
MCO_3 with calcite structure	0.969	80.31	−339.774
MCO_3 with aragonite structure	0.960	66.63	−326.105
Metal partitioning in carbonate phases			
	a^*_{MX}	β^*_{MX} (kcal/mol/Å)	b^*_{MX} (kcal/mol
M^{2+} in calcite	0.968	75.168	
M^{2+} in siderite	0.97	73.236	
M^{2+} in aragonite	0.96[a]	70.65	
M^{3+} in calcite	0.994	93.488	−329.68

[a] Fixed in regression. See discussion in the text.

$$\Delta G^0_{f,MX} = a_{MX}\Delta G^0_{n,M^{Z+}} + \beta_{MX} r_{M^{Z+}} + b_{MX} \quad (1)$$

where $\Delta G^0_{n,M^{Z+}}$ is the standard non-solvation energy of cation M^{Z+} (Sverjensky and Molling, 1992), $r_{M^{Z+}}$ is the ionic radius of cation M^{Z+} (Shannon and Prewitt, 1969), and a_{MX}, β_{MX}, and b_{MX} are constants for a given isostructural mineral family and are determined by fitting Eqn. 1 to experimental data. The non-solvation energy ($\Delta G^0_{n,M^{Z+}}$) can be calculated by:

$$\Delta G^0_{n,M^{Z+}} = \Delta G^0_{f,M^{Z+}} - \Delta G^0_{s,M^{Z+}} \quad (2)$$

where $\Delta G^0_{f,M^{Z+}}$ is the standard Gibbs free energy of formation of cation M^{Z+}; $\Delta G^0_{s,M^{Z+}}$ is the standard Gibbs free energy of solvation of cation M^{Z+} and can be calculated from the conventional Born solvation coefficient ($\omega_{M^{Z+}}$) (Shock and Helgeson, 1988):

$$\Delta G^0_{s,M^{Z+}} = \omega_{M^{Z+}}\left(\frac{1}{\varepsilon} - 1\right) \quad (3)$$

In the above equation, ε is the dielectric constant of water (78.47 at 25°C). The parameter $\omega_{M^{Z+}}$ is calculated by the following equation (Sverjensky and Molling, 1992):

$$\omega_{M^{Z+}} = \frac{166.027Z^2}{r_{M^{Z+}} + 0.94Z} - 53.87Z \quad \text{(kcal/mole)} \quad (4)$$

where Z is the charge of cation M^{Z+}.

Analogous to the well-known Hammett relationship for functional group substitution in organic compounds, Eqn. 1 captures the effect of cation substitution in a given mineral structure. Eqn. 1 can be cast in terms of mineral solubility products ($K_{sp,MX}$):

$$2.303 \log K_{sp,MX} + \Delta G^0_{f,M^{Z+}} = a_{MX}\Delta G^0_{n,M^{Z+}} + \beta_{MX} r_{M^{Z+}} + b'_{MX}$$
$$b'_{MX} = b_{MX} - \Delta G^0_{f,X^{Z-}} \quad (5)$$

where $\Delta G^0_{f,X^{Z-}}$ is the Gibbs free energy of formation of anion X^{Z-}.

The application of Eqn. 5 to divalent metal carbonate minerals is shown in Figure 1. The coefficients a_{MX}, β_{MX}, and b'_{MX} obtained by regression are listed in Table 1. As noted by Sverjensky and Molling (1992), the a_{MX} values for both calcite and aragonite are very close. With the obtained coefficients, the solubility products (K_{sp}) of divalent carbonate minerals with either a calcite or an aragonite structure are predicted (Table 2).

There might be other ways to correlate mineral solubility products with metal cation properties. For instance, solubility products could be correlated with $\Delta G^0_{f,M^{n+}}$ (Sverjensky 1984, 1985) or with $\Delta G^0_{f,M^{n+}}$ and $r_{M^{n+}}$. However, it is shown in Figure 2 that the correlation described by Eqn. 1 generally gives the best fit to experimental data. This correlation has been

Table 2. Correlation of solubility products of divalent metal carbonate minerals with metal cation properties. The experimental Log K_{sp} values are calculated from Gibbs free energy data given in Sverjensky and Molling (1992) and Drever (1982). The values for $r_{M^{2+}}$ and $\Delta G_{f,M^{2+}}$ metal cations are from Xu and Wang (1999c).

					Solubility product (Log K_{sp})			
					Calcite		Aragonite	
M^{2+}	$r_{M^{2+}}$ (Å)	$\Delta G_{s,M^{2+}}$ (kcal/mol)	$\Delta G_{f,M^{2+}}$ (kcal/mol)	$\Delta G_{n,M^{2+}}$ (kcal/mol)	Experimental	Predicted	Experimental	Predicted
Ca	1	−121.28	−132.12	−10.83	−8.49	−8.55	−8.35	−8.49
Mg	0.72	−145.8	−108.83	36.97	−8.14	−8.15		−5.59
Mn	0.82	−136.46	−55.2	81.26	−10.40	−10.11		−8.85
Fe	0.77	−141.04	−21.87	119.17	−10.53	−10.56		−9.05
Zn	0.745	−143.4	−35.17	108.23	−9.89	−10.05		−8.22
Cd	0.95	−125.31	−18.57	106.74	−11.18	−11.21		−11.42
Be	0.45	−175.03	−89.8	85.23		−3.71		1.23
Co	0.735	−144.36	−13	131.36		−10.46		−8.68
Ni	0.7	−147.76	−10.9	136.86		−10.15		−8.06
Cu	0.73	−144.84	15.55	160.39		−11.06		−9.42
Sr	1.16	−109.31	−133.72	−24.41		−7.61	−9.32	−9.06
Sn	1.11	−112.91	−6.63	106.28		−10.87		−12.68
Ba	1.36	−95.99	−132.73	−36.74		−5.32	−8.58	−8.69
Eu	1.17	−108.6	−129.1	−20.5		−7.63		−9.21
Hg	1.02	−119.72	39.36	159.08		−12.37		−13.63
Pb	1.18	−107.9	−5.79	102.11		−10.33	−12.83	−12.82
Ra	1.39	−94.14	−134.2	−40.06		−4.83		−8.49
Pd	0.8	−138.28	42.49	184.36		−9.66		−8.88
Pt	0.8	−138.28	54.8	196.67		−9.94		−9.24
UO_2	0.754	−142.45	−227.7	−85.25		−5.78		−2.77
PuO_2	0.76	−146.98	−183.5	−41.52		−6.82		−4.15

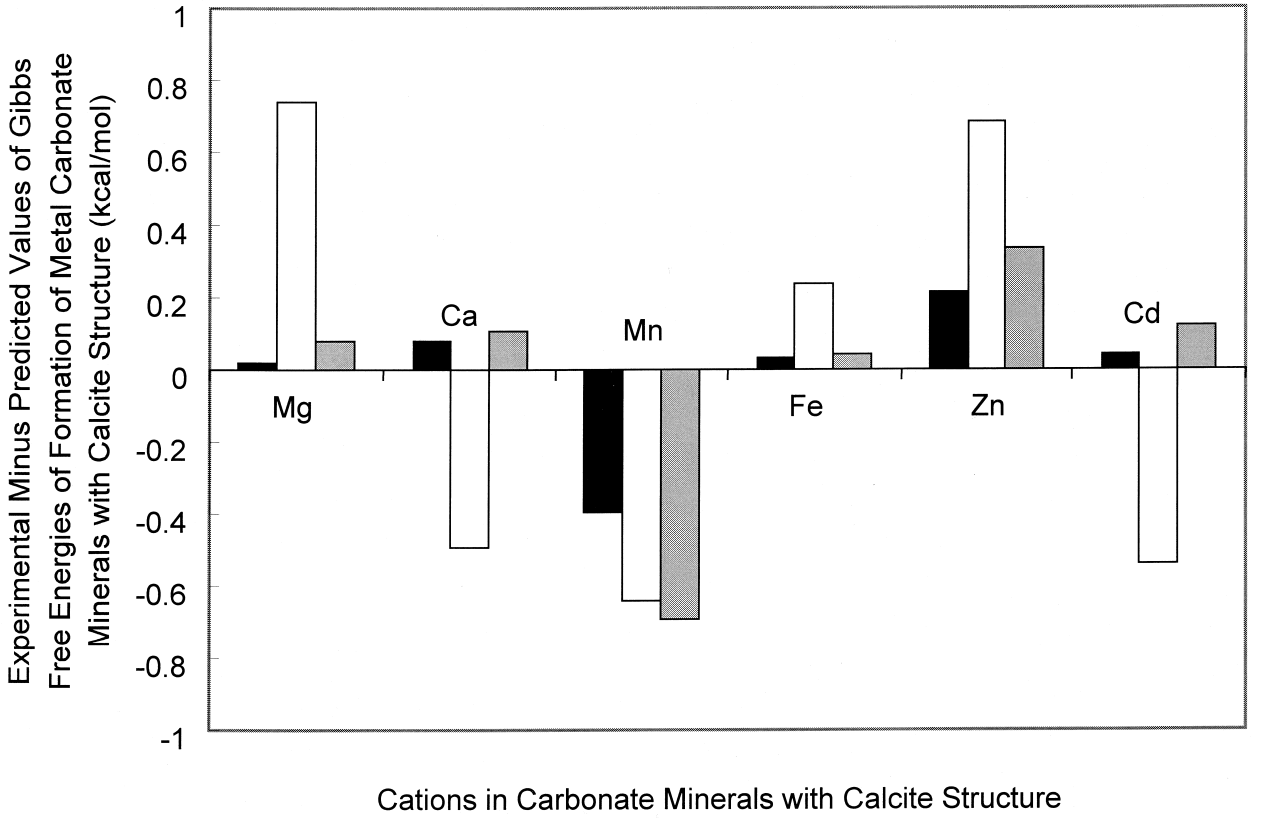

Fig. 2. Differences between predicted and experimental values of Gibbs free energies of formation of divalent metal carbonate minerals with calcite structure, for comparison of different correlation approaches: blank bars $-\Delta G^0_{f,MCO_3}$ vs. $\Delta G^0_{f,M^{n+}}$; gray bars $-\Delta G^0_{f,MCO_3}$ vs. $\Delta G^0_{f,M^{n+}}$ and $r_{M^{n+}}$; and black bars $-\Delta G^0_{f,MCO_3}$ vs. $\Delta G^0_{n,M^{n+}}$ and $r_{M^{n+}}$. The experimental values are taken from Sverjensky and Molling (1992). Notice that Eqn. 1 gives the best fit to the experimental data.

successfully applied to various mineral families (Xu et al., 1999; Xu and Wang, 1999a,b,c; Wang and Xu, 2000). In this paper, we want to extend the approach of Sverjensky and Molling (1992) to the correlation of metal partition coefficients.

3. ISOVALENT TRACE METAL PARTITIONING

3.1. Model Formulation

An isovalent metal partitioning process can be described by the following reaction:

$$M_H X + M^{Z+} = MX + M_H^{Z+} \tag{6}$$

where M^{Z+} and M_H^{Z+} are the substituent and host cations, respectively. The partition coefficient (K_d) of metal M_H^{Z+} between mineral $M_H X$ and an aqueous solution is defined as:

$$K_d = \left(\frac{X_{MX}}{X_{M_HX}}\right) \Big/ \left(\frac{m_{M^{Z+}}}{m_{M_H^{Z+}}}\right) \tag{7}$$

where X_{MX} and X_{M_HX} are the mol fractions of substituent and host metals in the solid phase, respectively; $m_{M^{Z+}}$ and $m_{M_H^{Z+}}$ are the molalities of cations M^{Z+} and M_H^{Z+} in the solution. The equilibrium of Eqn. 6 is described by the following mass-action expression:

$$-2.303RT \log \frac{X_{MX}\gamma_{MX} m_{M_H^{Z+}} \gamma_{M_H^{Z+}}}{X_{M_HX}\gamma_{M_HX} m_{M^{Z+}} \gamma_{M^{Z+}}} = \Delta G^0_{f,MX} + \Delta G^0_{f,M_H^{Z+}} - \Delta G^0_{f,M_HX} - \Delta G^0_{f,M^{Z+}} \tag{8}$$

where γ_i is the activity coefficient of species i, $\Delta G^0_{f,i}$ is the standard Gibbs free energy of formation of species i, R is the gas constant, and T is the temperature.

In a dilute solution, the activity coefficients of two isovalent cations are very close, and thus $\gamma_{M_H^{Z+}}/\gamma_{M^{Z+}} \approx 1$. In theory, the activity coefficients γ_{MX} and γ_{M_HX} depend on X_{MX} and X_{M_HX}, and this dependence can be described by the Margules equation (Anderson and Crerar 1993):

$$\begin{aligned} RT \ln \gamma_{MX} &= (2W_2 - W_1) X^2_{M_HX} + 2(W_1 - W_2) X^3_{M_HX} \\ RT \ln \gamma_{M_HX} &= (2W_1 - W_2) X^2_{MX} + 2(W_2 - W_1) X^3_{MX} \end{aligned} \tag{9}$$

where W_1 and W_2 are the Margules constants. Let us assume that a substituent metal is present only in a trace amount in the host mineral, i.e., $X_{MX} \rightarrow 0$ and $X_{M_HX} \rightarrow 1$. Under such conditions, from Eqn. 9, $\gamma_{MX} \rightarrow$ constant and $\gamma_{M_HX} \rightarrow 1$. In other words, the γ_{MX} in Eqn. 8 becomes independent of X_{MX} and is only a function of the properties of substituent cations. Based on these considerations, combining Eqn. 7 and Eqn. 8, we obtain:

Table 3. Experimental and predicted partition coefficients of divalent metals between carbonate minerals and aqueous solution. Experimental data in parenthesis are not used in the correlation analyses.

	Log K_d							
	Calcite		Siderite		Aragonite		Magnesite	Rhodochrosite
M^{2+}	Experimental[a]	Predicted	Experimental[b]	Predicted	Experimental[c]	Predicted	Predicted	Predicted
Ca		0	−1.08	−0.68		0	1.73	−0.67
Mg	−1.62	−1.44	−2.60	−2.59		−2.06	0	−2.40
Mn	1.31	0.92	0.91	−0.16		0.90	2.40	0
Fe	0.57	1.20		0		1.25	2.58	0.19
Zn	1.56	0.59		−0.64		0.49	1.97	−0.43
Cd	2.35	2.52		1.58		3.09	4.08	1.68
Be		−6.87		−8.48		−8.09	−5.72	−8.11
Co	0.92	0.97	−1.14	−0.31		0.98	2.32	−0.08
Ni		0.54	−0.92	−0.80		0.46	1.84	−0.55
Cu	1.38	1.57	(>2.60)	0.23		1.74	2.88	0.48
Sr	−1.42	−0.36		−0.78	0.10	0.10	1.53	−0.86
Sn		2.78		2.07		3.88	4.48	2.08
Ba	−1.77	−1.90		−2.02		−0.86	0.17	−2.22
Eu		−0.30		−0.71		0.21	1.59	−0.80
Hg		3.97		3.04		5.10	5.53	3.13
Pb		2.5		1.90		3.80	4.26	1.87
Ra	−1.84	−2.28		−2.34		−1.15	−0.17	−2.57
Pd		0.45		−0.83		1.00	1.78	−0.61
Pt		0.73		−0.57		1.36	2.05	−0.34
UO_2	(<−1.70)	−3.75		−4.64	(−0.52[4])	−5.00	−2.13	−4.52
PuO_2		−2.67		−3.62		−3.64	−1.09	−3.49

[1] Geometric average of K_d values compiled by Rimstidt et al. (1998, table 1a).
[2] From Thornber and Nickel (1996).
[3] From K_d data compiled by Curti (1997).
[4] Minimum value from Curti (1997).

$$-2.303RT \log K_d + \Delta G^0_{f,M^{z+}} = \Delta G^0_{f,MX} - 2.303RT \log \gamma_{MX} + b''_{M_HX} \quad (10)$$

where $b''_{M_HX} = \Delta G^0_{f,M_H^{z+}} - \Delta G^0_{f,M_HX}$ and depends only on the standard Gibbs free energies of formation of the host mineral and the host cation. Applying Eqn. 1 to the first two terms on the right side of Eqn. 10, which capture the effect of metal substitution, we have:

$$-2.303RT \log K_d + \Delta G^0_{f,M^{z+}} = a^*_{M_HX}\Delta G^0_{n,M^{z+}} + \beta^*_{M_HX} r_{M^{z+}} + b^*_{M_HX}. \quad (11)$$

Given a host mineral and a set of isovalent metals, the coefficients $a^*_{M_HX}$, $\beta^*_{M_HX}$, and $b^*_{M_HX}$ in Eqn. 11 are constants. The coefficient b''_{M_HX} in Eqn. 10 has been lumped into $b^*_{M_HX}$.

Eqn. 11 defines a linear free energy relationship that correlates metal partition coefficients with metal cation properties. Before applying this relationship to actual data, we need to consider an important constraint on Eqn. 11. This constraint is that for $M^{Z+} = M_H^{Z+}$, the predicted K_d using Eqn. 11 must be equal to 1. Notice that this constraint remains valid regardless of metal coprecipitation kinetics. Using this constraint to eliminate the coefficient $b^*_{M_HX}$ in Eqn. 11, we obtain:

$$-2.303RT \log K_d = a^*_{M_HX}(\Delta G^0_{n,M^{z+}} - \Delta G^0_{n,M_H^{z+}}) + \beta^*_{M_HX}(r_{M^{z+}} - r_{M_H^{z+}}) - (\Delta G^0_{f,M^{z+}} - \Delta G^0_{f,M_H^{z+}}). \quad (12)$$

Eqn. 12 only has two coefficients ($a^*_{M_HX}$ and $\beta^*_{M_HX}$) to be determined by a regression analysis.

3.2. Divalent Metal Partitioning between Carbonate Minerals and Aqueous Solutions

In this section, we apply Eqn. 12 to a set of data compiled by Rimstidt et al. (1998) and Curti (1997) for divalent metal partitioning between carbonate minerals and aqueous solutions. In cases where multiple sources of data exist (Rimstidt et al., 1998) (Table 1a), geometrically averaged values are used. The experimental data used for the regression analysis of Eqn. 12 are given in Table 3. In the regression, the experimental data that only specify open ranges (e.g., K_d values for UO_2^{2+} in calcite and Cu^{2+} in siderite) were not used, because the regression code we used was not able to handle this type of data. In addition, the K_d values for UO_2^{2+} were not used, because the nature of hexavalent uranium incorporation is not clear. The regression results are presented in Figure 3 and Table 1.

It is shown in Figures 3A and 3B that in spite of large uncertainties associated with original experimental data (e.g., the difference in reported K_d values for Cd can be more than one magnitude order; see Table 1a in Rimstidt et al., 1998), Eqn. 12 fits the data well, implying that a robust linear free energy correlation does exist between metal partition coefficients and metal cation properties. This correlation can be represented graphically by a linear line passing through the origin of coordinates (0, 0), corresponding to the host cation. As shown in Section 5, the correlation line moves like a seesaw anchored at the host cation, as the chemical system moves away from an equilibrium state.

By regression, the coefficients in Eqn. 12 are calculated to

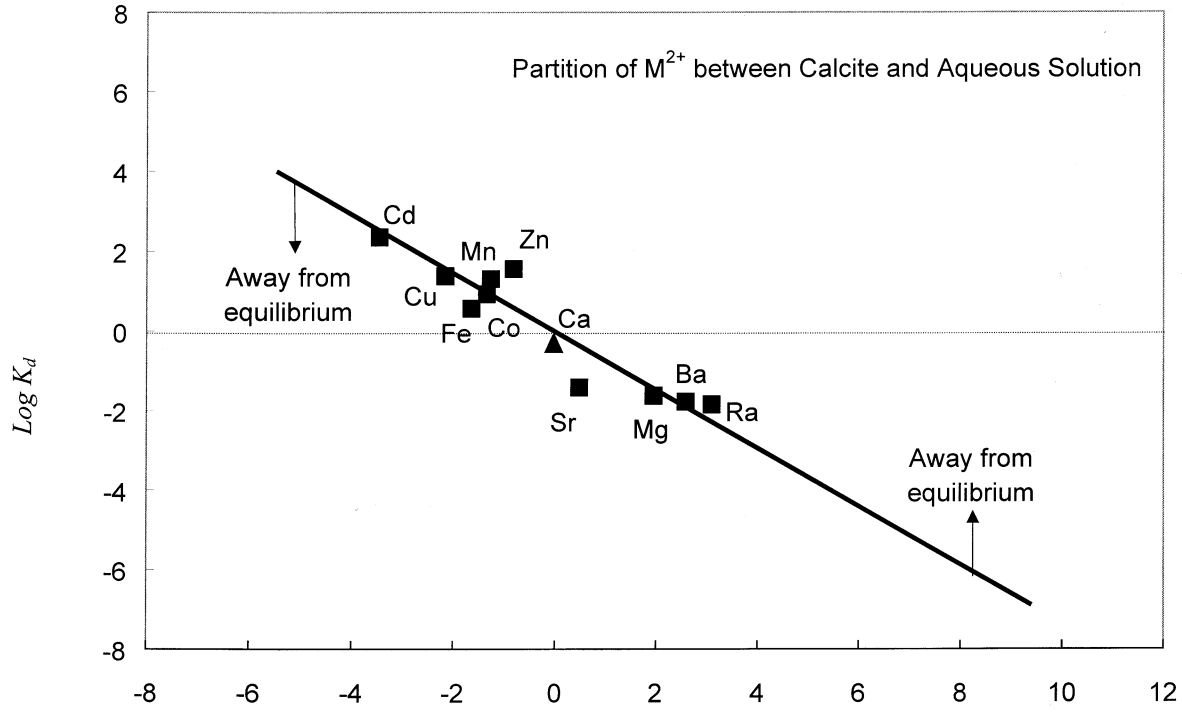

(a) $$0.968(\Delta G^0_{n,M^{2+}} - \Delta G^0_{n,Ca^{2+}}) + 75.17(r_{M^{2+}} - r_{Ca^{2+}}) - (\Delta G^0_{f,M^{2+}} - \Delta G^0_{f,Ca^{2+}})\ \text{(kcal/mol)}$$

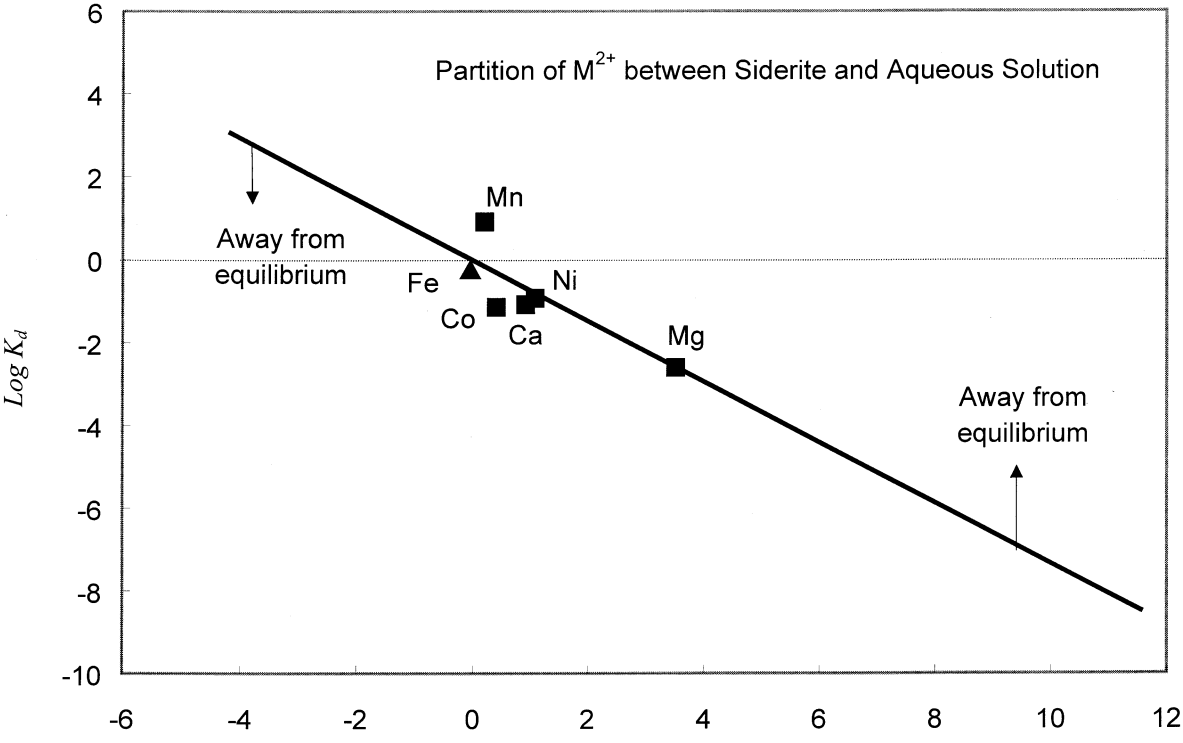

(b) $$0.971(\Delta G^0_{n,M^{2+}} - \Delta G^0_{n,Fe^{2+}}) + 73.24(r_{M^{2+}} - r_{Fe^{2+}}) - (\Delta G^0_{f,M^{2+}} - \Delta G^0_{f,Fe^{2+}})\ \text{(kcal/mol)}$$

Fig. 3. Linear correlation of divalent metal partition coefficients (K_d) with metal cation properties. For isovalent metal partitioning, a host metal, which has $K_d = 1$, serves as an invariant point for the correlation, and the kinetic effect on metal partitioning is described graphically by a "seesaw" line anchored at the host cation.

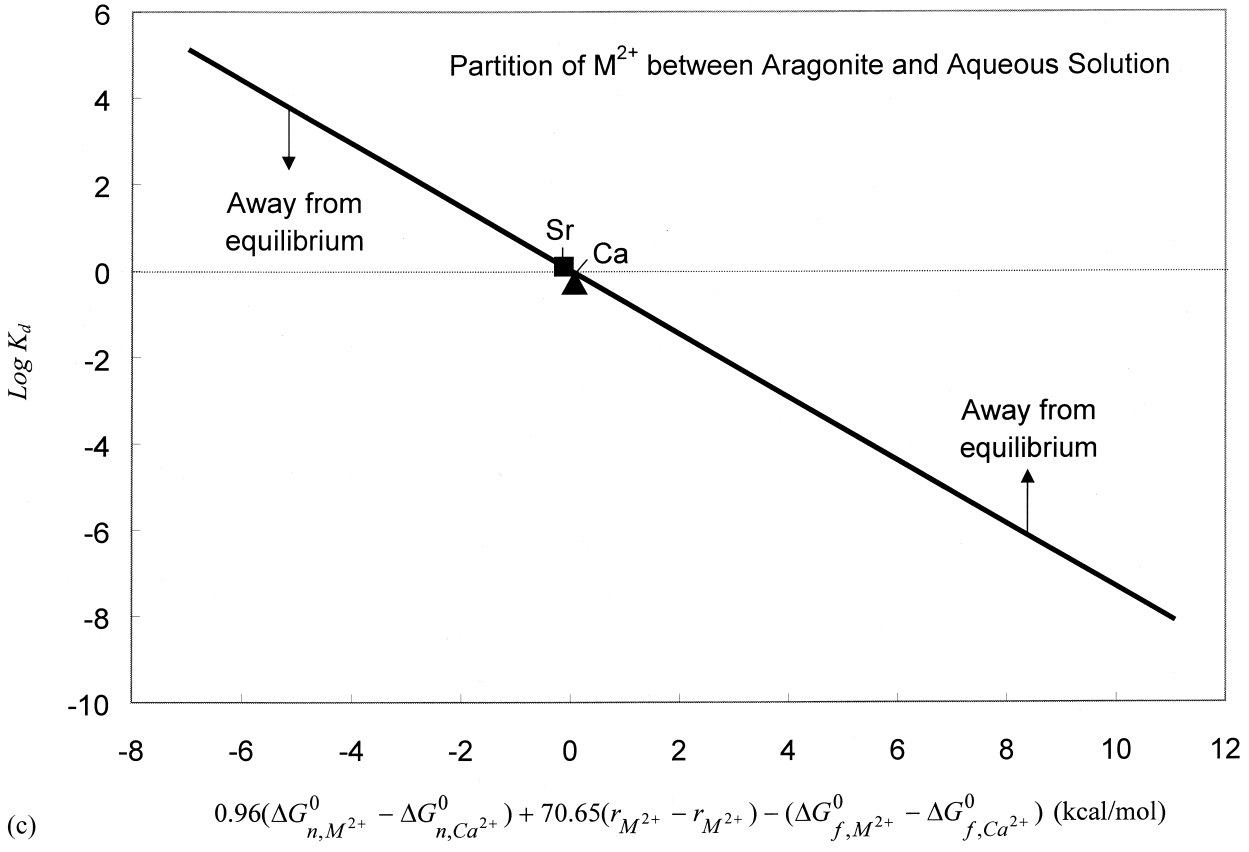

Fig. 3. (continued)

be: $a^*_{M_HX} = 0.968$, $\beta^*_{M_HX} = 75.17$ kcal/mol/Å for calcite, and $a^*_{M_HX} = 0.971$, $\beta^*_{M_HX} = 73.24$ kcal/mol/Å for siderite (Table 1). Notice that the coefficient $a^*_{M_HX}$ for both calcite and siderite are essentially the same, and furthermore they are the same as the a_{MX} value in Eqn. 5 for the pure mineral phases with a calcite structure (Table 1). This is not surprising, since Sverjensky and Molling (1992) have observed that the coefficient a_{MX} in Eqn. 5 is determined by the stoichiometry of minerals. Based on this observation, we have adopted $a^*_{M_HX} = 0.960$ for the divalent metal partitioning between aragonite and aqueous solutions. Using the K_d value of Sr determined by Kinsman and Holland (1969), the $\beta^*_{M_HX}$ value for divalent metal partitioning into aragonite is calculated to be 70.65 kcal/mol/Å. With the obtained $a^*_{M_HX}$ and $\beta^*_{M_HX}$ values, the partition coefficients of divalent metals for calcite, siderite, and aragonite are predicted (Table 3). The differences between predicted and experimental values are less than one logarithmic unit, with exceptions for Cu^{2+} in siderite and UO_2^{2+} in aragonite (Table 3). In comparison with a similar transition metal (Co^{2+}), the predicted K_d value for Cu^{2+} seems reasonable. We suspect the discrepancy between the measured and the predicted K_d values for Cu^{2+} in siderite is probably caused by Cu^{2+} reduction during coprecipitation. Unlike other cations listed in Table 3, UO_2^{2+} is a complex cation and the nature of its incorporation into carbonate mineral structure is still not clear. If uranium is incorporated as a free cation (U^{6+}) instead of a uranyl ion (UO_2^{2+}), our model would under predict the K_d value, since U^{6+} is highly charged and has a smaller radius. Apparently, to test this possibility, more K_d measurements, and especially some spectroscopic data, are needed.

It is shown in Eqn. 12 that a metal partition coefficient can be split into three terms, each with a clear physical meaning. The first term ($\Delta G^0_{n,M^{Z+}} - \Delta G^0_{n,M_H^{Z+}}$) is the difference between substituent and host cations in non-solvation free energy, and it characterizes the bonding ability of a substituent metal within a host mineral structure. The second term ($r_{M^{Z+}} - r_{M_H^{Z+}}$) accounts for the effect of metal radii. Theoretically, the lattice elastic strain energy created by the difference of radii between substituent and host cations can be modeled as a second order function of ($r_{M^{Z+}} - r_{M_H^{Z+}}$) (Gnanapragasam and Lewis, 1995; Purton et al., 1995; and Blundy et al., 1996). However, our modeling results show that the effect of metal radii on metal partitioning can be sufficiently represented by a linear term of ($r_{M^{Z+}} - r_{M_H^{Z+}}$). This may indicate that either the function of elastic strain energy can be approximated by a linear term of cation radii or the elastic strain energy alone does not fully capture the effect of cation radii on metal partitioning. Since the experimental data used in our model cover a wide range of cation radii (0.72–1.39 Å) (see Tables 2 and 3), the latter is more likely. Finally, the third term ($\Delta G^0_{f,M^{Z+}} - \Delta G^0_{f,M_H^{Z+}}$) characterizes the chemical potential difference between substituent and host cations in aqueous solutions at a standard state. This term is directly derived from a mass action expression (Eqn. 8).

For isovalent metal partitioning, a host cation plays a key role in our linear free energy correlation model. The constraint of $K_d = 1$ for the host cation reduces the degrees of freedom for fitting Eqn. 12 to experimental data. Additionally, the host cation serves as an invariant point for metal partitioning into a family of isostructural minerals. Notice that all terms on the right side of Eqn. 12 are expressed relative to the host cation. And also notice that the coefficients $a^*_{M_HX}$ and $\beta^*_{M_HX}$ are essentially the same for calcite and siderite, both having the calcite structure. These observations lead us to postulate that, given a set of substituent metals, host minerals from the same isostructural family have the same linear free energy relationship, i.e., the same $a^*_{M_HX}$ and $\beta^*_{M_HX}$ in Eqn. 12. We therefore choose $a^*_{M_HX} = 0.97$ and $\beta^*_{M_HX} = 74.0$ for magnesite ($MgCO_3$) and rhodochrosite ($MnCO_3$), both from the same isostructural family as calcite and siderite. The predicted partition coefficients of divalent metals for these two minerals are presented in Table 3. It can be seen that magnesite has the largest partition coefficients among isostructural minerals.

4. NON-ISOVALENT TRACE METAL PARTITIONING

4.1. Charge Compensation and Model Formulation

Non-isovalent metal partitioning is complicated by charge compensation. For example, depending on charge compensation mechanisms, the substitution of Ca^{2+} by a trivalent cation (M^{3+}) can be described by either:

$$CaCO_3 + 2/3M^{3+} = M_{2/3}CO_3 + Ca^{2+} \quad (13)$$

or:

$$2CaCO_3 + M^{3+} + Na^+ = MNa(CO_3)_2 + 2Ca^{2+} \quad (14)$$

if the charge is compensated by Na^+. In either case, a partition coefficient defined in Eqn. 7 is no longer a true equilibrium constant and dependent on solution chemistry, even if the activity coefficients of the relevant chemical species are neglected. In this section, we show that the linear free energy relationship developed above can also apply to non-isovalent metal partitioning. We use rare earth element (REE) partitioning between calcite and seawater as an example.

Because of the existence of a good correlation between REE and Na contents in calcite (Zhong and Mucci 1995), we here focus on Eqn. 14. The equilibrium of Eqn. 14 is described by:

$$-2.303RT \log \frac{X_{MNaCO_3}\gamma_{MNaCO_3}m^2_{Ca^{2+}}\gamma^2_{Ca^{2+}}}{X^2_{CaCO_3}\gamma^2_{CaCO_3}m_{M^{3+}}\gamma_{M^{3+}}m_{Na^+}\gamma_{Na^+}} = \Delta G^0_{f,MNaCO_3} + 2\Delta G^0_{f,Ca^{2+}} - 2\Delta G^0_{f,CaCO_3} - \Delta G^0_{f,M^{3+}} - \Delta G^0_{f,Na^+}. \quad (15)$$

Assuming that metal M^{3+} is present only in a trace amount in calcite, we have $X_{CaCO_3} \rightarrow 1$ and $\gamma_{CaCO_3} \rightarrow 1$. Unlike isovalent metal partitioning, the ratio of $\frac{m_{Ca^{2+}}\gamma^2_{Ca^{2+}}}{\gamma_{M^{3+}}m_{Na^+}\gamma_{Na^+}}$ in Eqn. 15 cannot cancel out. But nevertheless, for a fixed solution composition, this ratio is approximately a constant. In other words, the partition coefficients for non-isovalent metal substitution in principle depend on solution chemistry; therefore, the linear free energy correlation developed below can only apply to a set of data from the same set of experiments conducted under similar chemical conditions. Following the same procedure in Section 3.1 and applying Eqn. 1 to both $\Delta G^0_{f,MNaCO_3}$ and $\log \gamma_{MNaCO_3}$, we then obtain the linear free energy relationship for trivalent metal partitioning between calcite and aqueous solution:

$$-2.303RT \log K_d + \Delta G^0_{f,M^{3+}} = a^*_{CaCO_3}\Delta G^0_{n,M^{3+}} + \beta^*_{CaCO_3}r_{M^{2+}} + b^*_{CaCO_3} \quad (16)$$

which is similar to Eqn. 11.

4.2. Trivalent Metal Partitioning between Calcite and Aqueous Solution

We have applied Eqn. 16 to experimental data obtained by Zhong and Mucci (1995) (Table 4). It is shown in Figure 4 that the experimental data of partition coefficients of rare earth elements closely follow a linear free energy relationship defined by Eqn. 16. By regression, the coefficients $a^*_{CaCO_3}$, $\beta^*_{CaCO_3}$, and $b^*_{CaCO_3}$ are estimated to be 0.994, 93.488 kcal/mol/Å, and −329.68 kcal/mol, respectively. With the obtained coefficient values, the partition coefficients of trivalent metals between calcite and seawater are predicted (Table 4). The differences between predicted and experimental values are <0.4 logarithmic unit (Table 4).

Unlike isovalent metal partitioning, the point of $\log K_d = 0$ in Figure 4 is no longer corresponding to any actual cation, and instead it corresponds to a fictive cation. The properties of the fictive cation, in principle, can be calculated if the partition coefficients are measured for two host minerals from the same isostructural family.

5. NON-EQUILIBRIUM METAL PARTITIONING

5.1. Rate Dependence of Partition Coefficients

Metal partition coefficients generally depend on the rate of host mineral precipitation (Lorens 1981; Dromgoole and Walter 1990; Tesoriero and Pankow 1996). This dependence usually displays the following features:

- Seesaw behavior: The partition coefficients of divalent cations in calcite can either increase or decrease with calcite precipitation rate, depending on whether their values are <1 or >1 (Lorens 1981; Dromgoole and Walter 1990; Tesoriero and Pankow 1996) (Fig. 5). Also notice that the partition coefficient of the host cation must be equal to 1 regardless of coprecipitation kinetics. Therefore, as illustrated in Figure 3, the effect of mineral precipitation kinetics makes the linear free energy correlation line move around the host cation (Ca^{2+}) just like a seesaw. As the precipitation rate increases, that is, as the system moves away from equilibrium, the correlation line becomes more horizontal.
- Asymptotic behavior: As shown in Figure 5, a partition coefficient approaches a plateau as the rate of host mineral precipitation increases. Tesoriero and Pankow (1996) suggested that at high precipitation rates, the ratio of M^{2+}/Ca^{2+} in calcite would approach what was found in solution. If this were the case, the partition coefficient would approach 1. As shown in Figure 5, however, the asymptotic K_d values are never close to 1.

Table 4. Experimental and predicted partition coefficients of trivalent metals between calcite and aqueous solution.

M^{3+}	$r_{M^{3+}}$ (Å)	$\Delta G_{s,M^{3+}}$ (kcal/mol)	$\Delta G_{f,M^{3+}}$ (kcal/mol)	$\Delta G_{n,M^{3+}}$ (kcal/mol)	Log K_d	
					Experimental[a]	Predicted
La	1.14	−218.51	−164.00	54.51	3.62	3.62
Ce	1.07	−225.39	−161.60	63.79	3.53	3.42
Nd	1.04	−228.41	−160.60	67.81	3.18	3.28
Sm	1.00	−232.52	−159.10	73.42	3.06	3.04
Gd	0.97	−235.65	−158.60	77.05	2.75	2.82
Dy	0.92	−240.99	−158.70	82.29	2.41	2.35
Yb	0.86	−247.81	−153.00	94.81	1.85	1.53
Pr	1.06	−226.39	−162.60	63.79	3.49	3.37
Eu	0.98	−234.60	−137.30	97.30	2.89	3.00
Tb	0.93	−239.91	−159.50	80.41	2.51	2.45
Ho	0.91	−242.08	−161.40	80.68	1.99	2.23
Er	0.89	−244.26	−159.90	84.36	1.85	2.02
Pm	1.06	−226.39	−158.00	68.39		3.40
Lu	0.85	−248.94	−159.40	89.54		1.36
U	1.12	−220.45	−124.40	96.05		3.77
Pu	1.08	−224.39	−138.15	86.24		3.58
Np	1.10	−222.41	−123.59	98.82		3.72
Am	1.07	−225.39	−143.19	82.20		3.51
Cr	0.62	−276.92	−51.50	225.42		−2.75
Fe	0.65	−273.11	−4.12	268.99		−1.81
Co	0.63	−275.01	32.03	307.04		−1.65
Ga	0.62	−276.28	−38.00	238.28		−2.22
Ti	0.76	−259.08	−83.60	175.48		0.50
V	0.64	−273.74	−57.90	215.84		−1.83
Sc	0.81	−253.25	−140.20	113.05		1.05
Tl	0.95	−237.77	51.30	289.07		3.63
Bi	0.96	−236.71	19.79	256.50		3.57
In	0.81	−253.25	−23.40	229.85		1.60
Y	0.92	−240.99	−163.80	77.19		2.33
Tm	0.87	−246.59	−159.90	86.69		1.70

[a] Compiled by Rimstidt et al. (1998).

- For highly-charged cations such as REE (rare earth elements), the rate dependence of partition coefficients has not been observed (Zhong and Mucci, 1995).

An explanation has been proposed for the seesaw effect (Rimstidt et al., 1998), but a theoretical model that can account for all three features mentioned above is still lacking.

5.2. Boundary Layer Effect

The high rate of host mineral precipitation may deplete cation concentrations at a crystallization surface, thus creating a boundary layer that has a different cation ratio than the bulk solution (Wang and Merino, 1992; Tiller, 1991). Rimstidt et al., (1998) used this concept to explain the seesaw feature of the rate dependence of partition coefficients. The effect of boundary layer on M^{2+} partitioning into calcite is described by the following mass balance equations (Wang and Merino, 1992):

$$R_p = \lambda(m^{\infty}_{Ca^{2+}} - m^{0}_{Ca^{2+}}) \tag{17}$$

$$R_p K_d \frac{m^{0}_{M^{2+}}}{m^{0}_{Ca^{2+}}} = \lambda(m^{0}_{M^{2+}} - m^{0}_{M^{2+}}) \tag{18}$$

where R_p is the precipitation rate of calcite (mol/cm^2/s); m^0_i and m^∞_i are the concentrations of cation i at the crystallization surface and in the bulk solution, respectively; λ is the rate constant for mass exchange between the bulk solution and the boundary layer by diffusion. Solving Eqn. 17 and 18 for $m^0_{M^{2+}}$ and $m^0_{Ca^{2+}}$, we obtain:

$$\frac{m^{0}_{M^{2+}}}{m^{0}_{Ca^{2+}}} = \frac{m^{\infty}_{M^{2+}}}{m^{\infty}_{Ca^{2+}} + (K_d - 1)\dfrac{R_p}{\lambda}} = \frac{m^{\infty}_{M^{2+}}}{m^{\infty}_{Ca^{2+}}} \cdot \frac{1}{1 + (K_d - 1)R'_p} \tag{19}$$

where $R'_p = R_p/\lambda m^{\infty}_{Ca^{2+}}$, a scaled calcite precipitation rate ranging from 0 to 1, according to Eqn. 17. Dividing both sides of Eqn. 19 by X_{MCO_3}/X_{CaCO_3}, and using Eqn. 7, we obtain:

$$K'_d = \frac{K_d}{1 + (K_d - 1)R'_p} \tag{20}$$

where

$$K'_d = \left(\frac{X_{MCO_3}}{X_{CaCO_3}}\right) \Big/ \left(\frac{m^{\infty}_{M^{2+}}}{m^{\infty}_{Ca^{2+}}}\right) \tag{21}$$

K'_d is the apparent partition coefficient actually measured in experiments. Eqn. 20 predicts that if the effect of boundary layer were the main factor controlling the rate dependence of partition coefficient, the measured partition coefficient (K'_d) would approach 1 as calcite precipitation rates increase (i.e., $R'_p \rightarrow 1$). However, experimental data have shown that the partition coefficients of divalent cations in calcite never asymptotically approach 1 as the calcite precipitation rates increase

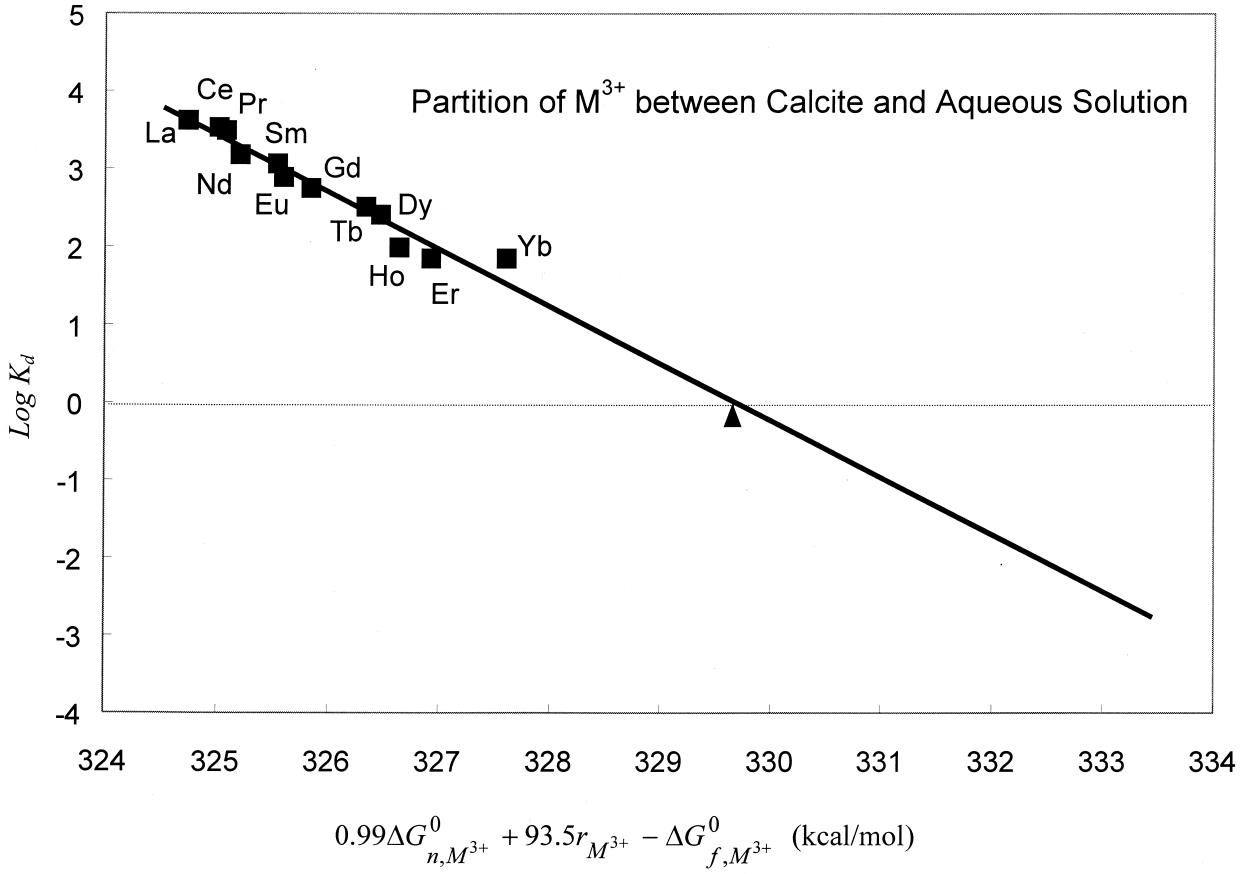

Fig. 4. Linear correlation of trivalent metal partition coefficients (K_d) with metal cation properties. Notice that for non-isovalent metal partitioning, the point of $K_d = 1$ is no longer corresponding to any actual metal, instead it corresponds to a fictitious element.

(Fig. 5). Thus, the boundary layer effect may partly account for the observed seesaw feature of divalent metal partitioning in calcite, but this effect alone is unable to explain the observed asymptotic behavior of partition coefficients. Furthermore, the boundary layer effect cannot explain the lack of rate dependence for some highly charged cations.

5.3. From Adsorption to Coprecipitation: A Conceptual Model

In this section, we propose a conceptual model that can explain all three features of the rate dependence of partition coefficients summarized in Section 5.1. Our model takes into account the effect of surface adsorption on metal partitioning. We here use metal partitioning between calcite and aqueous solutions as an example.

As illustrated in Figure 6, several intermediate steps are involved in a whole metal partitioning process. We focus only on metal adsorption and subsequent incorporation. We assume that metal adsorption at a calcite-water interface remains in equilibrium with aqueous solution. Thus, the ratio of $[M^{2+}]/[Ca^{2+}]$ in the adsorbed layer is constant, as long as the composition of aqueous solution is fixed. Since a mineral-water interface is a transition zone between aqueous solution and solid, for equilibrium metal partitioning we expect that:

$$\left.\frac{[M^{2+}]}{[Ca^{2+}]}\right|_{\text{solution}} < \left.\frac{[M^{2+}]}{[Ca^{2+}]}\right|_{\text{adsorbed}} < \left.\frac{[M^{2+}]}{[Ca^{2+}]}\right|_{\text{solid}} \quad \text{for } K_d > 1$$

$$\left.\frac{[M^{2+}]}{[Ca^{2+}]}\right|_{\text{solid}} < \left.\frac{[M^{2+}]}{[Ca^{2+}]}\right|_{\text{adsorbed}} < \frac{[M^{2+}]}{[Ca^{2+}]^{\text{solution}}} \quad \text{for } K_d < 1 \tag{22}$$

We further assume that metal partitioning is limited by the incorporation of adsorbed cations into the bulk calcite structure. For the incorporated metals to equilibrate with the adsorbed cations, a certain relaxation time (T_R) is required. When the precipitation rate of calcite $R_p > \rho\sqrt{D/T_R}$, where ρ is the molar density of calcite (mol/cm^3) and D is the diffusion coefficient of metal cation in calcite (cm^2/s), the kinetic effect on metal partitioning must be considered. The observed trace metal sector zoning in calcite (Reader and Grams, 1987; Temmam et al., 2000) is good evidence for non-equilibrium metal partitioning. The actual amount of metal incorporated into calcite is determined by two driving forces: chemical potential and physical trapping. As the calcite precipitation rate increases, the physical trapping gradually takes over the chemical potential

force, and consequently the ratio of $[M^{2+}]/[Ca^{2+}]$ in calcite approaches that in the adsorbed layer. As a result, from Eqn. 20, depending on whether K_d is larger or smaller than 1, the K_d value can either decrease or increase with calcite precipitation rate. An asymptotic K_d value is thus determined by the ratio of $[M^{2+}]/[Ca^{2+}]$ in the adsorbed layer instead of the bulk solution. This explains why K_d values never approach 1 as the calcite precipitation rate increases.

For highly charged cations such as REE, because of their large adsorption coefficients (Zhong and Mucci, 1995), we expect that for equilibrium metal partitioning:

$$\left.\frac{[M^{3+}]}{[Ca^{2+}]}\right|_{\text{adsorbed}} \approx \left.\frac{[M^{3+}]}{[Ca^{2+}]}\right|_{\text{solid}}. \tag{23}$$

Therefore, the effect of calcite precipitation rate on partition coefficients is minimal and hard to observe.

The conceptual model summarized above provides a reasonable explanation for the observed features of the rate dependence of metal partition coefficients. The concept can be possibly tested by careful analyses using near-surface sensitive spectroscopic techniques, such as X-ray photoelectron spectroscopy (XPS) (e.g., Stipp et al., 1992), combined with quantitative modeling. The related work is in progress, and the results will be reported elsewhere.

6. DISCUSSION AND MODEL APPLICATION

The correlation model developed in this paper is a natural extension of work of Sverjensky (1984), Sverjensky and Molling (1992), and Rimstidt et al. (1998). However, our model has several unique aspects. The following is a comparison of our model with those of Sverjensky (1984) and Rimstidt, et al., (1998):

- The radius difference between substituent and host cations can have a significant contribution to metal partitioning (e.g.,, Gnanapragasam and Lewis, 1995; Rimstidt et al., 1998) (Fig. 5). Using the $\beta^*_{M_HX}$ value obtained by regression analysis (Table 1), we estimate that this contribution can be up to 34 kcal/mol for divalent metal partitioning in calcite. Both models of Sverjensky (1984) and Rimstidt et al. (1998) do not explicitly account for the effect of cation radii; thus, the application of these models is limited to cations that have similar radii as host cations. As realized by Sverjensky (1984), the application of his model is limited preferably to cations with radius differences $< 10\%$. In contrast, our model accounts simultaneously for the effect of cation radii ($r_{M^{z+}} - r_{M_H^{z+}}$), the bonding ability of substituent cations within a host mineral structure ($\Delta G^0_{n,M^{z+}} - \Delta G^0_{n,M_H^{z+}}$), and the chemical potential difference between substituent and host cations in solution ($\Delta G^0_{f,M^{z+}} - \Delta G^0_{f,M_H^{z+}}$). Therefore, our model can apply to a whole range of cations, as demonstrated in Figures 3 and 4. For example, for divalent metal partitioning in calcite, our model fits all experimental data with a single straight line (Fig. 3A). In contrast, to fit the same data set, the model of Rimstidt et al. (1998) needs to invoke two correlation lines to accommodate the scattering of data points, and actually, the line for large cations seems arbitrarily introduced (Rimstidt et al., 1998) (Fig. 2).
- The model of Rimstidt et al. (1998) has another limitation. The model requires solubility product data for pure mineral phases, many of which are not available. For example, as mentioned in Section 1.0, large divalent cations such as Pb^{2+}, Ra^{2+}, Ba^{2+}, Sr^{2+}, Sn^{2+}, and Eu^{2+} never form stable carbonate minerals with a calcite structure, and the solubility products of these "fictitious" mineral phases are difficult to obtain. In principle, this limitation could be overcome by using the solubility products predicted by the method summarized in Section 2.0. In fact, we did try this approach, but found that the partition coefficients of divalent metals in calcite were poorly correlated with the predicted solubility products. The lack of the expected correlation again indicates that the effect of cation radii must be explicitly considered in the correlation of metal partition coefficients.
- The model of Sverjensky (1984) correlated the Gibbs free energies of formation of pure carbonate mineral phases ($\Delta G^0_{f,MX}$) only with $\Delta G^0_{f,M^{z+}}$. Sverjensky and Molling (1992) made a significant improvement in this correlation by explicitly considering the effect of the Born solvation energies and the radii of cations. The significance of this improvement is demonstrated in Figure 2. Our model further extends work of Sverjensky and Molling (1992) by assuming that both terms, $\Delta G^0_{f,MX}$ and log γ_{MX} in Eqn. 10, can be correlated to the non-solvation energies ($\Delta G^0_{n,M^{z+}}$) and the radii ($r_{M^{z+}}$) of metal cations, respectively.
- No previous models have identified the importance of the physical constraint that the partition coefficient of a host cation must be equal to 1 for isovalent metal partitioning. This constraint remains valid regardless of host mineral precipitation rate and plays an important role in our model. It reduces the degree of freedom for model fitting and serves as an invariant point for metal partitioning into a family of isostructural minerals. Our work indicates that host minerals from the same isostructural family have the same linear free energy relationship for a given set of substituent metals. Therefore, our model can potentially be used to correlate a family of isostructural minerals, instead of only a single solid phase as previous models have done. Due to the existence of the invariant point, the kinetic effect on a linear free energy relationship can be described graphically by a seesaw line anchored at the host cation (Fig. 3).
- Our model could apply to elevated temperatures if there were sufficient experimental K_d data available to parameterize the coefficients $a^*_{M_HX}$ and $\beta^*_{M_HX}$ in Eqn. 12. Both $a^*_{M_HX}$ and $\beta^*_{M_HX}$ would then become a function of temperature. As shown in Section 3.2, the coefficient $a^*_{M_HX}$ in Eqn. 12 is very close to the a_{MX} in Eqn. 5 for pure mineral phases (see Table 1). Since the temperature dependence of thermodynamic properties of pure minerals and metal cations can be predicted using the models developed by Helgeson et al. (1978, 1981), theoretically, both the first and the last terms on the right side of Eqn. 12 can be calculated. However, the evaluation of the $\beta^*_{M_HX}$ term in Eqn. 12 requires actual K_d measurements at elevated temperatures, which are currently lacking. Furthermore, as demonstrated above, the $\beta^*_{M_HX}$ term (i.e., the effect of cation radii) can have a significant contribution to overall metal partitioning. Therefore, under current circumstances one should be cautious to extend our model to elevated temperatures. The same caution should be taken for both models of Sverjensky (1984) and Rimstidt et al. (1998).

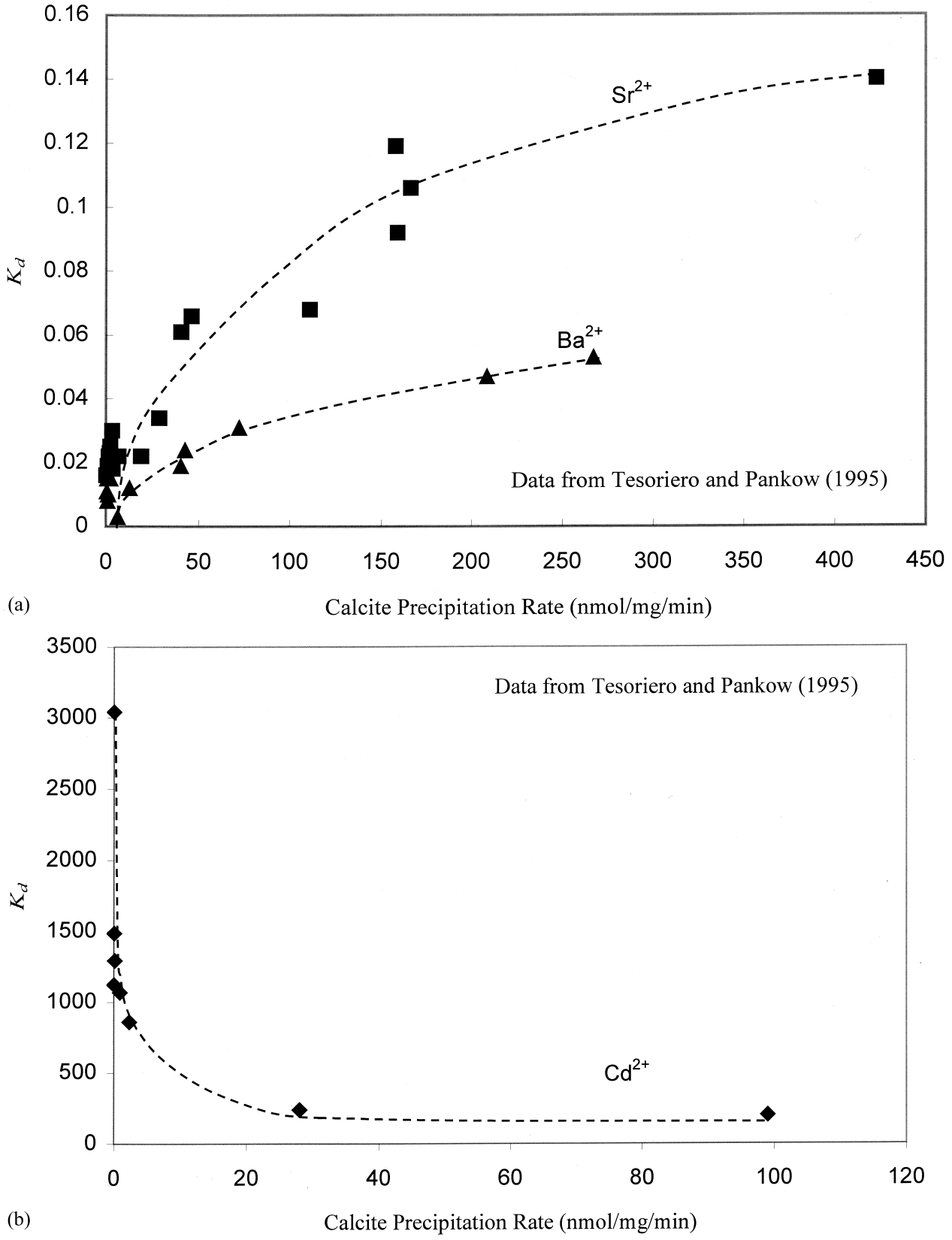

Fig. 5. Rate dependence of partition coefficients of divalent metal in calcite. Notice that the partition coefficients can either increase or decrease with calcite precipitation rates, depending on whether their values are less or greater than 1. As the calcite precipitation rates increase, the partition coefficients approach certain plateau values, which are never close to 1.

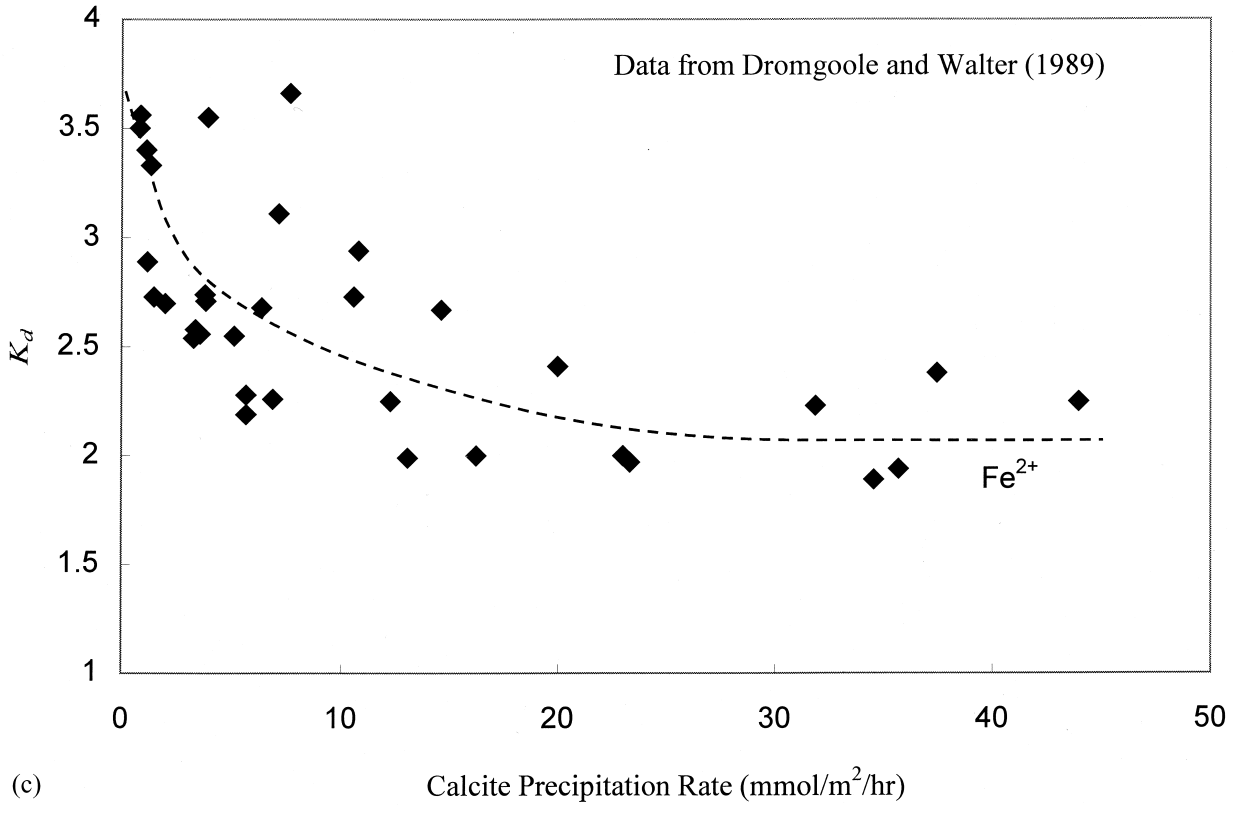

Fig. 5. (continued)

The predictions of these two models for elevated temperatures could be valid only for metal cations with very similar radii.

6.1. Immobilization of Heavy Metals by MgO Backfill in WIPP: An Example of Geochemical Engineering

Geochemical engineering makes use of optimized geochemical processes for the solution of environmental problems (Schuiling, 1998; Brady and Kozak, 1995; van Gaans, 1998). Waste containment and contaminant immobilization are an active aspect of current geochemical engineering, in which the prediction of metal partitioning between aqueous and solid phases plays an important role in engineering design (e.g., Curti, 1997; Rimstidt et al., 1998). As an example of our model applications, we here discuss the implication of the partition coefficients predicted above to the immobilization of heavy metals (including radionuclides) by MgO backfill in the Waste Isolation Pilot Plant (WIPP).

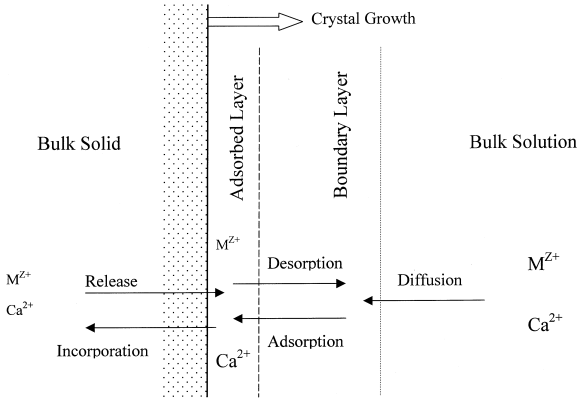

Fig. 6. A conceptual model for explaining the rate dependence of metal partition coefficients. Metal partitioning is assumed to be limited by the incorporation of absorbed cations into mineral structure. As the rate of host mineral precipitation increases, the ratio of substituent to host cation in a solid approaches what is in the adsorbed layer.

The WIPP is a deep geologic repository located in a salt bed in southern New Mexico and is designed by the U.S. Department of Energy to demonstrate the safe and permanent disposal of design-basis transuranic wastes. According to waste inventory estimates, a large quantity of organic material is expected to be emplaced in the WIPP, and they will be degraded potentially by halophilic or halotolerant microorganisms in the repository, thus generating a large amount of CO_2 (Wang et al., 1997):

$$C_6H_{10}O_5 + H_2O \rightarrow 3\,CH_4 + 3\,CO_2. \quad (24)$$

To mitigate the effect of microbial CO_2 generation on the WIPP performance, a sufficient amount of MgO is added to the repository as a backfill to control repository conditions through the following reactions (Bynum et al., 1998):

$$MgO + H_2O \rightarrow Mg(OH)_2 \quad (25)$$

$$Mg(OH)_2 + CO_2 \rightarrow MgCO_3 + H_2O. \quad (26)$$

The reaction shown in Eqn. 26 will buffer CO_2 fugacity at $\sim 10^{-7}$ atm and pmH at 9 to 10. Under such conditions, radionuclide solubility will become minimal, and therefore, potential releases of radionuclides to the environment will be reduced significantly (Wang et al., 1997; Bynum et al., 1998).

Due to the microbial reaction and the emplacement of MgO backfill, it is anticipated that a large quantity of magnesite (or other magnesium carbonate minerals) will potentially be formed in the WIPP. Our model prediction (Table 3) indicates that the heavy metal partition coefficients for magnesite are usually at least one magnitude order higher than those for other carbonate minerals, and thus, magnesite is a good scavenger for heavy metals. Therefore, in the WIPP, MgO backfill will not only reduce radionuclide solubility but also possibly immobilize radionuclides by coprecipitation. Furthermore, because of its high coprecipitation capability, MgO is probably a good choice as backfill material for nuclear waste isolation, as compared with other materials such as CaO-based materials (e.g., Brady and Kozak, 1995).

7. CONCLUSIONS

We have developed a linear free energy correlation model that correlates metal partition coefficients with the properties of corresponding metal cations. According to the model, a metal partition coefficient can be expressed as a linear combination of $(\Delta G^0_{n,M^{z+}} - \Delta G^0_{n,M_H^{z+}})$, which characterizes the bonding ability of a substituent metal, $(r_{M^{z+}} - r_{M_H^{z+}})$, which accounts for the effect of metal radii, and $(\Delta G^0_{f,M^{z+}} - \Delta G^0_{f,M_H^{z+}})$, which represents the chemical potential difference between substituent and host cations in solution. We have applied our model to both isovalent and non-isovalent metal partitioning between carbonate minerals and aqueous solutions. The model closely fits experimental data, demonstrating the robustness of the proposed linear free energy relationship. Using the model, we have predicted the partition coefficients of divalent and trivalent metals between various carbonate minerals and aqueous solutions. The differences between the predicted and experimental values are generally <1 logarithmic unit for divalent cations and <0.4 logarithmic unit for trivalent cations. Magnesite is predicted to have the largest partition coefficients among the carbonate minerals with a calcite structure and therefore, can be a good scavenger for toxic metals. The implication of this prediction to heavy metal immobilization in the WIPP deep geologic repository is discussed.

For isovalent metal partitioning, the constraint of $K_d = 1$ for a host metal plays an important role in our linear free energy correlation. It reduces the degrees of freedom for model fitting and serves as an invariant point for metal partitioning into a family of isostructural minerals. It is postulated that host minerals from the same isostructural family have the same linear free energy relationship, as long as the relationship is expressed as a function of the differences in cation properties between substituent and host metals. For non-isovalent metal partitioning, a similar linear free energy relationship is also developed by taking into account the detailed charge compensation mechanisms.

The kinetic effect on metal partitioning can be described graphically by a seesaw line anchored at a host cation. To explain the rate dependence of partition coefficients, we have proposed a conceptual model that relates metal partitioning to surface adsorption. The model suggests that as the rate of host mineral precipitation increases, the ratio of substituent to host cation in a solid approaches what is in the adsorbed layer. The model also explains why no rate dependence has been observed for the partition coefficients of highly charged cations.

The linear free energy correlation developed in this paper provides a useful tool for systematizing existing experimental data and for predicting unknown partition coefficients. Combined with reactive transport modeling (e.g., Wang and Papenguth, 2000), this correlation approach will allow us to systematically evaluate the effect of coprecipitation on toxic metal migration and bioavailability in subsurface environments.

Acknowledgments—We thank Associate Editor E. Merino, J. D. Rimstidt, and two anonymous reviewers for their constructive review comments. We also thank M. A. Martell and D. Guerin at Sandia National Laboratories for their help. Sandia is a multi-program laboratory operated by Sandia Corporation, a Lockheed Martin Co., for the United States Department of Energy (US DOE) under Contract DE-AC04 to 94AL85000. This research is partly supported by the DOE through the Waste Isolation Pilot Plant (WIPP) project. Xu thanks NSF of China (No. 49928201) for partial support of this study.

Associate editor: E. Merino

REFERENCES

Anderson G. M. and Crerar D. A. (1993) *Thermodynamics in Geochemistry: The equilibrium Model*. Oxford University Press, New York.

Barnaby R. and Rimstidt J. D. (1989) Redox conditions of calcite cementation interpreted from Mn and Fe contents of authigenic calcites. *GSA Bull.* **101,** 795–804.

Blundy J. D. and Wood B. J. (1994) Prediction of crystal-melt partition coefficients from elastic moduli. *Nature* **372,** 452–454.

Blundy J. D., Wood B. J., and Davies A. (1996) Thermodynamics of rare earth element partitioning between clinopyroxene and melt in the system CaO-MgO-Al_2O_3-SiO_2. *Geochim. Cosmochim. Acta* **60,** 359–364.

Brady P. V. and Kozak M. W. (1995) Geochemical engineering of low level radioactive waste in cementitious environments. *Waste Management* **15,** 293–301.

Bynum R. V., Stockman C. T., Papenguth H. W., Wang Y., Peterson A. C., Krumhansl J. L., Nowak E. J., Cotton J., Patchet S. J., and Chu M. S. Y. (1998) Identification and evaluation of appropriate backfills for the Waste Isolation Pilot Plant (WIPP). In *International Workshop on the Uses of Backfill in Nuclear Waste Repositories, May 1998, Carlsbad, NM* (ed. D. G. Bennett, H. W. Papenguth, M. S. Y. Chu, D. A. Galson, S. L. Duerden, and M. L. Matthews), Environmental Agency & US DOE, Carlsbad, NM. pp. 2-178–2-187.

Curti E. (1997) Coprecipitation of radionuclides: Basic concepts, literature review and first applications. *PSI Bericht* Nr. 97-10, Paul Scherrer Institut, Würenlingen, Switzerland.

Curti E. (1999) Coprecipitation of radionuclides with calcite: Estimation of partition coefficients based on a review of laboratory investigations and geochemical data. *Applied Geochemistry* **14,** 433–445.

Davis J. A., Fuller C. C., and Cook A. D. (1987) A model for trace metal sorption processes at the calcite surface: Adsorption of Cd^{2+} and subsequent solid solution formation. *Geochim. Cosmochim. Acta* **51,** 1477–1490.

Drever J. I. (1982) *The Geochmistry of Natural Waters* Prentice-Hall, Englewood Cliffs, N.J.

Dromgoole E. and Walter L. (1990) Iron and manganese incorporation into calcite: Effects of growth kinetics, temperature and solution chemistry. *Chem. Geol.* **81,** 311–336.

Frank J. R., Carpenter A. B., and Oglesby T. W. (1982) Cathodolumi-

nescence and composition of calcite cement in the Tau Sauk Limestone (Upper Cambrian), Southeast Missouri. *J. Sediment. Petrol.* **52,** 631–638.

Gnanapragasam E. K. and Lewis B. G. (1995) Elastic strain energy and the distribution coefficient of radium in solid solutions with calcium salts. *Geochim. Cosmochim. Acta* **59,** 5103–5111.

Grover G. A. Jr. and Read J. F. (1983) Paleoaquifer and deep burial related cements defined by regional cathodoluminescent patterns, Middle Ordovician carbonates, Virginia. *AAPG Bull.* **67,** 1275–1303.

Helgeson H. C., Delaney J. M., Nesbitt H. W., and Bird D. K. (1978) Summary and critique of the thermodynamic properties of rock-forming minerals. *Am. J. Sci.* **278A,** 229 pp.

Helgeson H. C., Kirkham D. H., and Flowers G. C. (1981) Theoretical prediction of the thermodynamic behavior of aqueous electrolytes at high pressures and temperatures. IV. Calculation of activity coefficients, osmotic coefficients, and apparent molal and standard and relative properties to 5 kb and 600°C. *Am. J. Sci.* **281,** 1241–1516.

Kinsman D. J. J. and Holland H. D. (1969) The co-precipitation of cations with $CaCO_3$-IV. The co-precipitation of Sr^{2+} with aragonite between 16° and 90°C. *Geochim. Cosmochim. Acta* **33,** 1–17.

Lorens R. B. (1981) Sr, Cd, Mn, and Co distribution coefficients in calcite as a function of calcite precipitation rate. *Geochim. Cosmochim. Acta* **45,** 553–561.

McIntire W. (1963) Trace element partition coefficients-a review of theory and applications to geology. *Geochim. Cosmochim. Acta* **27,** 1209–1264.

Meyers W. J. (1974) Carbonate cement stratigraphy of the Lake Valley Formation (Mississipian), Sacramento Mountains, New Mexico. *J. Sediment. Petrol.* **44,** 837–861.

Meyers W. J. (1978) Carbonate cements: Their regional distribution and interpretation in Mississipian limestones of southwest New Mexico. *Sedimentology* **25,** 371–399.

Mucci A. and Morse J. W. (1983) The incorporation of Mg^{2+} and Sr^{2+} into calcite overgrowths: Influences of growth rate and solution composition. *Geochim. Cosmochim. Acta* **47,** 217–233.

Purton J. A., Allan N. L., Blundy J. D., and Wasserman E. A. (1995) Isovalent trace element partitioning between minerals and melts: A computer simulation study. *Geochim. Cosmochim. Acta* **60,** 4977–4987.

Reeder R. J and Grams J. C. (1987) Sector zoning in calcite cement crystals: Implications for trace-element distribution in carbonates. *Geochim. Cosmochim. Acta* **51,** 187–194.

Rimstidt J. D., Balog A., and Webb J. (1998) Distribution of trace elements between carbonate minerals and aqueous solutions. *Geochim. Cosmochim. Acta* **62,** 1851–1963.

Schuiling R. D. (1998) Geochemical engineering: Taking stock. *J. Geochem. Explor.* **62,** 1–28.

Shannon R. D. and Prewitt C. T. (1969) Effective ionic radii in oxides and fluorides. *Acta Cryst.* **B25,** 925–946.

Shock E. L. and Helgeson H. C. (1988) Calculation of the thermodynamic and transport properties of aqueous species at high temperatures: Correlation algorithms for ionic species and equation of state predictions to 5 Kb and 1000°C. *Geochim. Cosmochim. Acta* **52,** 2009–2036.

Speer J. A. (1983) Crystal chemistry and phase relations of orthorhombic carbonates. In *Carbonates: Mineralogy and Chemistry* (ed. R. J. Reeder), *Rev. Mineral.* **11,** 145–225.

Stipp S. L., Hochella M. F., Parks G. A., and Leckie J. O. (1992) Cd^{2+} uptake by calcite, solid-state diffusion, and formation of the solid-solution: Interface processes observed with near-surface sensitive techniques (XPS, LEED, and AES). *Geochim. Cosmochim. Acta* **56,** 1941–1954.

Sverjensky D. A. (1984) Prediction of Gibbs free energies of calcite-type carbonates and the equilibrium distribution of trace elements between carbonates and aqueous solutions. *Geochim. Cosmochim. Acta* **48,** 1127–1134.

Sverjensky D. A. (1985) The distribution of divalent trace elements between sulfides, oxides, silicates and hydrothermal solutions: I. Thermodynamic basis. *Geochim. Cosmochim. Acta* **49,** 853–864.

Sverjensky D. A. and Molling P. A. (1992) A linear free energy relationship for crystalline solids and aqueous ions. *Nature* **356,** 231–234.

Temmam M., Paquette J., and Vali H. (2000) Mn and. Zn incorporation into calcite as a function of chloride aqueous concentration. *Geochim. Cosmochim. Acta* **64,** 2417–2430.

Tesoriero A. and Pankow J. (1996) Solid solution partitioning of Sr^{2+}, Ba^{2+}, and Cd^{2+} to calcite. *Geochim. Cosmochim. Acta* **60,** 1053–1063.

Thornber M. R. and Nickel E. H. (1976) Supergene alterations of sulfides. III. The composition of associated carbonates. *Chem. Geol.* **17,** 45–72.

Tiller W. A. (1991) *Science of Crystallization: Microscopic Interfacial Phenomena*, Cambridge University Press.

Van Gaans P. F. M. (1998) The role of modeling in geochemical engineering—a (re)view. *J. Geochem. Explor.* **62,** 41–55.

Veizer J. (1983) Chemical diagenesis of carbonates: Theory and application of trace element technique. In *Stable Isotopes in Sedimentary Geology* (ed. M. A. Arthur), pp. 3/1–3/100, Society of Economic Paleontologists and Mineralogists.

Wang Y., Brush L. H., and Bynum R. V. (1997) Use of MgO to mitigate the effect of microbial CO_2 production in the Waste Isolation Pilot Plant. *WM '97 Proc., March., 2–6: 1997*, Paper 36-15 (CD-ROM), Tucson, Arizona.

Wang Y. and Merino E. (1992) Dynamic model of oscillatory zoning of trace elements in calcite: Double layer, inhibition, and self-organization. *Geochim. Cosmochim. Acta* **56,** 587–596.

Wang Y. and Papenguth H. W. (2000). Kinetic modeling of microbially-driven chemistry of radionuclides in subsurface environments: Coupling transport, microbial metabolism and geochemistry. *J. Contam. Hydrol.* (in press).

Wang Y. and Xu H. (2000). Thermodynamic stability of actinide pyrochlore minerals in deep geologic repository environments. *Mat. Res. Soc. Symp. Proc., Scientific Basis for Nuclear Waste Management,* **XXIII,** 367–372.

Xu H. and Wang Y. (1999a) Use of linear free energy relationship to predict Gibbs free energy of formation of zirconolite phases ($MZrTi_2O_7$ and $MHfTi_2O_7$). *J. Nucl. Mater.* **275,** 211–215.

Xu H. and Wang Y. (1999b) Use of linear free energy relationship to predict Gibbs free energy of formation of pyrochlore phases ($CaMTi_2O_7$). *J. Nucl. Mater.* **275,** 216–220.

Xu H. and Wang Y. (1999c) Use of linear free energy relationship to predict Gibbs free energy of formation of MUO_4 phases. *Radiochim. Acta* **87,** 37–40.

Xu H., Wang Y., and Barton L. L. (1999) Application of a Linear Free Energy Relationship to crystalline solids of MO_2 and $M(OH)_4$ phases. *J. Nucl. Mater.* **273,** 343–346.

Zhong S. and Mucci A. (1995) Partitioning of rare earth elements (REE's) between calcite and seawater solutions at 25°C and 1 atm and high dissolved REE concentrations. *Geochim. Cosmochim. Acta* **59,** 443–453.